Photoionization of helium between the $N=2$ and $N=5$ thresholds of He^+: Partial differential cross sections

Yuhai Jiang,[1,2] Jun Yan,[3] Jiaming Li,[3,4] Jinfeng Sun,[1,2] and Lingde Wan[2]
[1]*CCAST (World Laboratory), P. O. Box 8730, Beijing 100080, China*
[2]*Department of Physics, Henan Normal University, Xinxiang 453002, China**
[3]*Center of Atomic and Molecular Sciences, Tsinghua University, Beijing 100084, China*
[4]*Institute of Physics, Chinese Academy of Science, Beijing 100080, China*
(Received 12 April 1999; published 17 February 2000)

Photoionization excitation of helium has been performed employing the *R*-matrix method with a 20-term target representation for incident photon energies between the $N=2$ and $N=5$ thresholds (69–76.8 eV) of the He^+ ion. Partial differential cross sections for photoionization leaving the He^+ ion in the $N=2,3,4$ levels at emission angles $0°$ and in the $N=2$ level $90°$ are provided. Our results to He^+ in the $N=2$ state give fairly good agreement with the available experimental data and theoretical calculations below the $N=3$ threshold. Between the $N=3$ and $N=5$ thresholds of the He^+ ion, our results for He^+ in the $N=2,3,4$ states still agree with experiment qualitatively.

PACS number(s): 32.80.Fb, 32.80.Dz

I. INTRODUCTION

Photoionization excitation of helium to $He^+(N)$ states is an example of a two-electron system that has been extensively studied for electron correlation effects. The fact that direct photoionization and autoionization from highly correlated doubly excited states can interfere makes these studies a challenging task for theoreticians, particularly in the evaluation of partial cross sections to different $He^+(N)$ ionic levels. For this reason helium is an important system for testing various theoretical approaches to the phenomenon of electron correlation. In the past 20 years, a lot of experimental [1–6] and theoretical [7–19] effort has been focused on the calculation of total cross sections, asymmetry parameters β and resonance properties of photoionization of helium leaving He^+ ion in an excited state. In this article, we are concerned with the partial differential cross sections (DCS) of photoionization of helium from the $N=2$ to $N=5$ thresholds of He^+ (about 69–77 eV). It is well known that differential cross sections for photoionization are much more sensitive than the total cross sections to small deficiencies in the wave functions. The shapes of the DCS for photoionization are slightly more complex and depend on the ionization channels that are considered. It is an extremely demanding task to calculate the photoionization spectra at photon energies above 75 eV because of the presence of multitudes of resonances and perturbations by other series. In addition, exploring these high-lying doubly excited states is important for consolidating our present understanding of the electron-electron correlations. This yields vital information concerning what takes place at even higher energies and how to describe double ionization near threshold (at 79 eV). Theoretical reproduction of the experimental findings is a first step that we need to achieve for extracting relevant information and before we explore even higher energy regimes. The angular distributions of photoionization to the $He^+(N=2)$ state at $90°$ [20] angle and the $He^+(N=2,3,4)$ states at $0°$ [21] angle have been studied by Zubek *et al.* in experiments with linearly polarized light over the photon energy 69–77 eV. In this energy region, photoionization is dominated by abundant autoionization states from doubly excited states of helium. Theoretically, Sánchez and Martín [9] in 1992 reported the differential cross sections $d\sigma_{N=2}/d\Omega$ of photoionization for $\theta=0°$ and $90°$ angles at incident photon energy 69–73 eV (between the $N=2$ and $N=3$ thresholds of the He^+ ion) using a Feshbach partitioning of the final-state wave function and an L^2 representation of the coupled continuum states. No other partial DCSs for photoionization to $He^+(N=2,3,4)$ are found above a photon energy of 73 eV in the literature. In the present paper, we employ the *R*-matrix approach [22–25] to calculate the DCS for photoionization of helium leaving He^+ in the $N=2,3,4$ states at $\theta=0°$, and the $N=2$ state at $\theta=90°$, below the $N=5$ threshold of the He^+ ion. In Sec. II, we describe *R*-matrix theory and how these target states are determined. In Sec. III, we detail the *R*-matrix calculations and discuss our results of partial DCS for photoionization of helium to the $He^+(NL)$ states. Our conclusions are given in Sec. IV. Atomic units and energy in Rydbergs are used throughout this paper if not specified.

II. *R*-MATRIX METHOD OF PHOTOIONIZATION

For helium, the spin-orbit effects may be safely neglected, so that the LS coupling is quite adequate. In this paper, the partial cross sections (DCSs) for photoionization are calculated for the following process:

$$h\upsilon + \mathrm{He}(1s^2)^1S \rightarrow [\mathrm{He}^+(NL) + e(nl)]^1P^o. \qquad (1)$$

For photoelectrons $e(nl)$ ejected from unpolarized target atoms by linear polarized radiation, the partial DCS for photoionization, in the electric dipole approximation, can be written [22]

*Address for correspondence.

$$\frac{d\sigma_{NL}}{d\Omega}=\frac{\sigma_{NL}}{4\pi}[1+\beta_{NL}P_2(\cos\theta)], \tag{2}$$

where N and L are, respectively, the principle and orbital angular quantum numbers of the residual electron, θ is the angle between the photoelectron momentum and the incident polarization direction, and σ_{NL} are the partial cross sections into the NL state of the residual ion. $P_2(\cos(\theta))$ is the second Legendre polynomial. β_{NL}, the asymmetry parameters, are defined in Ref. [22]. Experimental work provides the asymmetry parameter β_N for the angular distributions of the total photoelectron emission to the $N=2,3,4$ levels, which are related to the β_{NL} in the following way:

$$\beta_N=\frac{\sum_L \sigma_{NL}\beta_{NL}}{\sum_L \sigma_{NL}}. \tag{3}$$

For example, in the case of helium, a resultant β_2 parameter is measured which is the weighted average of β_{2s} and β_{2p} given by

$$\beta_2=\frac{\sigma_{2s}\beta_{2s}+\sigma_{2p}\beta_{2p}}{\sigma_{2s}+\sigma_{2p}}. \tag{4}$$

R-matrix theory starts by partitioning configuration space into two regions by a sphere of radius a centered on the target nucleus. In the internal region $r\leqslant a$, electron exchange and correlation between the scattered electron and the N-electron target are important. In order to determine the $(N+1)$-electron solution in the internal region, energy-independent basis states Ψ_k are introduced, which are expanded in the form

$$\Psi_k=A\sum_{ij} c_{ijk}\bar{\phi}_i(x_1,\ldots,x_N;\hat{r}_{N+1}\sigma_{N+1})\frac{1}{r_{N+1}}u_{ij}(r_{N+1}) + \sum_j d_{jk}\chi_j(x_1,\ldots,x_{N+1}), \tag{5}$$

where A is the antisymmetrization operator which accounts for electron exchange between the target electrons and the free electron. $\bar{\phi}_i$ are channel functions of the target terms that are included in the close-coupling (CC) expansion and are coupled to the angular and spin functions of the scattered electron. χ_j in the second sum, which vanish at the surface of the internal region, are formed from the bound orbitals of the $(N+1)$-electron system and are included to ensure completeness of the total wave function. The c_{ijk} and d_{jk} coefficients in Eq. (5) are determined by diagonalizing the $(N+1)$-electron Hamiltonian.

The continuum orbitals u_{ij} in Eq. (5), for each angular momentum l_i, are normally obtained by solving the model single-channel scattering problem

$$\left(\frac{d^2}{dr^2}-\frac{l_i(l_i+1)}{r^2}+V_0(r)+k_{ij}^2\right)u_{ij}(r)=\sum_n \Lambda_{ijn}P_{nl_i}(r), \tag{6}$$

subject to the fixed boundary conditions

$$u_{ij}(0)=0, \tag{7}$$

$$\left(\frac{a}{u_{ij}(a)}\right)\left(\frac{du_{ij}}{dr}\right)_{r=a}=0. \tag{8}$$

The Lagrange multipliers Λ_{ijn} ensure that the continuum orbitals are orthogonal to the bound orbitals $P_{nl_i}(r)$ of the same angular momentum. $V_0(r)$ is a zero-order potential chosen to be the static potential of target. k_{ij}^2 and a are the eigenvalues and the radius of the sphere defining the internal region, respectively.

The orbital functions $P_{nl}(r)$ are expressed in Slater-type analytic form

$$P_{nl}(r)=\sum_{jnl} C_{jnl}r^{P_{jnl}}\exp(-\xi_{jnl}r) \tag{9}$$

and they satisfy the orthonormality conditions

$$\int_0^\infty P_{nl}(r)P_{n'l'}(r)dr=\delta_{nn'}. \tag{10}$$

C_{jnl}, ξ_{jnl}, and P_{jnl} are Clementi-Roetti parameters [26]. In external region, the colliding electron is outside the atom and a set of coupled differential equations satisfied by the reduced radial wave functions are solved subject to the boundary conditions as $r\to\infty$. The two regions are linked by the R matrix on the boundary $(r=a)$ [22].

The R-matrix method uses the same target orbitals in dealing with initial and final $(N+1)$-electron states in photoionization calculations. The choice of a good and final $(N+1)$-electron basis in the first sum of Eq. (5) as well as a good configuration-interaction (CI) expansion for each target state is very crucial. In the present work, the CC expansion of the He^+ target is represented by 20 states obtained from the configurations nl, $n=1,2,3,4,5$ and $l=s,p,d,f,g$ as well as $\bar{6}s$, $\bar{6}p$, $\bar{6}d$, $\bar{6}f$, $\bar{6}g$, $\bar{6}h$. The $1s$-$5g$ are hydrogenic wave functions of the He^+ ion and they limit the present calculations to the resonances below the $N\leqslant 5$ thresholds. The $\bar{6}l$ are polarized correlation orbitals of He^+ and represent electron correlation optimized on the ground state using the CIVPOL code [27]. In building up the set of radial functions, we have ensured that Eq. (10) is satisfied for P_{nl} with $n'\leqslant n$ by choosing $k=n-l$ in Eq. (9). Thus, the coefficients C_{jnl} in Eq. (9) are uniquely determined by the orthonormality conditions (10). When we fix the integers P_{jnl}, only the ξ_{jnl} are treated as variational parameters. The optimized parameters are shown in Table I.

The polarized orbitals included in the target states make Eq. (5) converge faster and provide better ground state energy. It's effect on photoionization cross sections and resonance properties for $^1P^o$ doubly excited states of the He

TABLE I. Radial function parameters for the He^+ targets.

Orbital (nl)	C_{jnl}	P_{jnl}	ξ_{jnl}
$1s-5g$		Hydrogenic orbitals	
$\overline{6s}$	3.72615	1	0.99478
	−12.31193	2	1.01114
	15.65776	3	0.99832
	−7.40524	4	0.99084
	0.68349	5	0.48055
	−0.37439	6	0.37308
$\overline{6p}$	1.57314	2	2.22668
	−1.28440	3	1.69799
	1.60044	4	0.50277
	−2.42762	5	0.47997
	1.06946	6	0.45202
$\overline{6d}$	1.00608	3	3.69850
	−0.14955	4	1.02029
	0.21028	5	0.42455
	−0.17955	6	0.41004
$\overline{6f}$	0.99998	4	4.78402
	−0.01674	5	0.57790
	0.01191	6	0.44364
$\overline{6g}$	1.00000	5	5.95148
	−0.00036	6	0.43459

atom has been discussed in detail [18]. Here, it improves the agreement between the results in length and velocity forms [18]. A severe but good test for the choice of target terms is provided by the calculation of the ground state energy. The ground state has an energy of $E=-4+I$ obtained from the variational principle, where I is the ionization energy. Table II lists ionization energies I calculated by the use of different sets of target functions in Refs. [18,29,30]. Our results provide an energy of −1.80243 Ry for I compared to the nonrelativistic limit −1.8074 Ry [28], and show better results than other calculations using different target terms in Table II. Table III provides the effective quantum numbers for the $^1S^e$ and the $^1P^o$ states of the e^-+He^+ system compared

TABLE II. Ionization energies I for the He ground state $(1s^2)^1S$.

States included in expansion	I	Reference
$1s$	−1.7450	Ref. [29]
$1s,\overline{2p},\overline{3d}$	−1.7817	Ref. [29]
$1s,2s',\overline{2p},2p',\overline{3d}$	−1.8007	Ref. [29]
$1s,2s,2p,\overline{3p},\overline{3d}$	−1.7868	Ref. [30]
$1s,2s,2p,3s,3p,3d$	−1.7732	Ref. [18]
$1s,2s,2p,\ldots,4f$	−1.7741	Ref. [18]
$1s,2s,2p,\ldots,5g$	−1.7742	Ref. [18]
$1s,2s,2p,3s,3p,3d,\overline{4s},\overline{4p},\overline{4d}$	−1.7908	Ref. [18]
$1s,2s,2p,\ldots,5g,\overline{6s},\ldots,\overline{6h},$	−1.8024	present work
Pekeris's result	−1.8074	Ref. [31]

with the R-matrix calculations of Fernley *et al.* [30] and the experimental values of Moore [31]. It is seen that our results are very close to experimental and theoretical ones for each series. Another check on the convergence of our CI expansion is provided by the agreement of our results in the length and velocity formulations, which will be seen and discussed below. All these show that the most important physics is included by using the present target state expansion.

III. CALCULATIONS AND RESULTS

Initial bound states, excited states, and final continuum states of the $(N+1)$-electron system are calculated on the same footing using the R-matrix method with the following parameters: R-matrix radius $a=43.4\ a_0$, orbital angular momenta of the scattered electrons $l\leqslant 5$, and $N=70$ continuum basis functions for each orbital angular momentum. Employing the theory described above, we have evaluated the partial differential cross sections of photoionization leaving the residual He^+ ion in the $N=2,3,4$ states and the results are shown in Figs. 1–9 along with available experimental data. The spectrum is dominated by resonance structures due to series of doubly-excited autoionizing states, for which the classification scheme of Herrick and Sinanoglu [32] is the most appropriate. Here the simplified nomenclature N,K_n has been used, where N and n are the principal quantum numbers of the inner and outer electron respectively and K is the collective quantum number.

In Fig. 1, we present the DCS $d\sigma_{N=2}/d\Omega$ of photoionization for $\theta=90°$ between the $N=2$ and $N=5$ thresholds (69–76.8 eV) in the length and velocity forms. Figure 2 shows our convoluted values using Gaussian function with energy resolution of 60 meV. The DCS for photoionization into the $He^+(N=2)$ state for $\theta=90°$ has been obtained experimentally as a continuous function of photon energy by Zubek *et al.* [20] with linearly polarized light. Figures 3 and 4 present our results of the DCS for photoionization to $He^+(N=2)$, but for $\theta=0°$, and our convoluted calculations, with resolution 50 meV, along with experimental measurements of Zubek *et al.* [21]. As seen in Figs. 1–4, our calculations in the length and velocity forms are in good agreement. In general, as seen in Figs. 1–4, the present DCSs of photoionization to the $He^+(N=2)$ state are in fairly good agreement in the positions and shapes of observable autoionization resonances. Between the $N=2$ and $N=3$ thresholds (about 69–73 eV), Sánchez and Martín [9] in 1992 have reported their theoretical calculations on the DCS for photoionization to the $He^+(N=2)$ state for $\theta=90°$ and $\theta=0°$ based on Feshbach partitioning of the final-state wave function and an L^2 representation of the coupled continuum states. Their results, not convoluted, were compared directly with Zubek's measurements in Fig. 6 of Ref. [9]. Since we cannot collect their exact theoretical data, a direct comparison between two approaches is not given in the present work. However, we may learn from Fig. 6 ($\theta=90°$) and Fig. 5 ($\theta=0°$) in Ref. [9] that their calculations agree well with ours and with the experimental data on the shapes for the strong $3,1_n$ ($n=3,4,5,6$) resonance states. One difference found is that their positions of the $3,1_n$ states shift to higher

TABLE III. Effective quantum numbers of helium, experimental values of Moore [33] and the theoretical calculations employing *R* matrix by Fernley *et al.* [30] (in brackets).

	$1sns(^1S^e)$		$1snp(^1P^o)$	
n	Present calc. (Ref. [30])	Expt. [33]	Present calc. (Ref. [30])	Expt. [33]
1	0.74485(0.7481)	0.7439		
2	1.85205(1.8579)	1.8509	2.01016(2.0101)	2.0095
3	2.85799(2.8637)	2.8568	3.01203(3.0120)	3.0113
4	3.85972(3.8657)	3.8585	4.01254(4.0125)	4.0118
5	4.86051	4.8593	5.01276	5.0120
6	5.86090	5.8596	6.01287	6.0121
7	6.86115	6.8598	7.01294	7.0121
8	7.86131	7.8602	8.01299	8.0117
9	8.86142	8.8595	9.01302	9.0117
10	9.86149	9.8596		

energies compared with the measurements of Zubek *et al.* and the present calculations. In addition, the present theoretical results give some high-lying resonance states $3,1_n$ ($n \geqslant 7$) in Figs. 1 and 3. These are not seen in the experimental results due to a lower resolution of 50~60 meV. Between the $N=2$ and $N=3$ thresholds, the spectrum includes five series of resonance which, in the independent-electron limit, correspond to configurations of the form $3snp$, $3pns$, $3pnd$, $3dnp$, and $3dnf$. The lowest member of the much weaker $3,1_n$ series can also be seen clearly in Zubek's measurements and is in good agreement with the two theoretical values. It can be observed that there is a strong anisotropy between 71.0 and 72.0 eV in Figs. 1 for 90° and 3 for 0° (see also Ref. [9]). The magnitudes of this effect are sensibly increased in measured cross sections due to limited experimental resolution, which prevents the detection of all the resonance peaks. The very narrow $3,2_n$ resonance states are seen clearly from Figs. 1 and 3 in the present work and Sánchez and Martín's calculations (Figs. 1 and 6 in Ref. [9]). Due to the lower energy resolution of the photoelectron (60 and 50 meV), the resonance series $(3,2_n)$ were not observed in the experiments of Zubek *et al.* Between the $N=3$ and $N=5$ thresholds (about 73–76.8 eV) other calculations of the DCS of photoionization to the $He^+(N=2)$ state at 90° and 0° are have not been found in the literature. Figures 1 and 2 show that the present calculations reproduce the experimentally observed strong series corresponding to $4,2_n$ and $5,3_n$ converging to the $He^+(N=4)$ and $He^+(N=5)$ ionization thresholds. The $4,0_4$ state (located at about 74.3 eV) observed in experiments is also reproduced in present results and is in good agreement with the positions and shapes obtained from Figs. 1 and 2. Apart from that, the present calculations of the DCS for photoionization can provide rich resonance series whose properties will be discussed and studied in detail, along with higher resolution experiments, in future work.

The present and measured DCSs for photoionization to the $He^+(N=2)$ and $He^+(N=3)$ states at $\theta=0°$ below the $He^+(N=4)$ threshold are shown in Figs. 5 and 6, respectively. Parts (b) and (c) in Figs. 5 and 6 represent, respectively, the relative measurement of Ref. [21] and the present results convoluted using a Gaussian function (resolution of

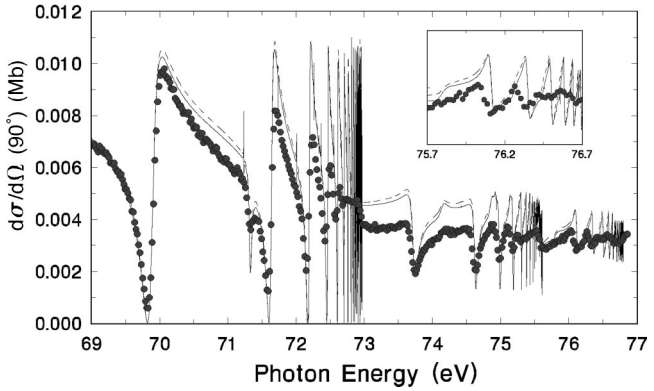

FIG. 1. Differential cross sections for photoionization into the $He^+(N=2)$ state at $\theta=90°$ at the photon energy range 69–76.8 eV. Solid line, our results in the length form; dashed line, our results in the velocity form; solid circles, experimental data in Ref. [20].

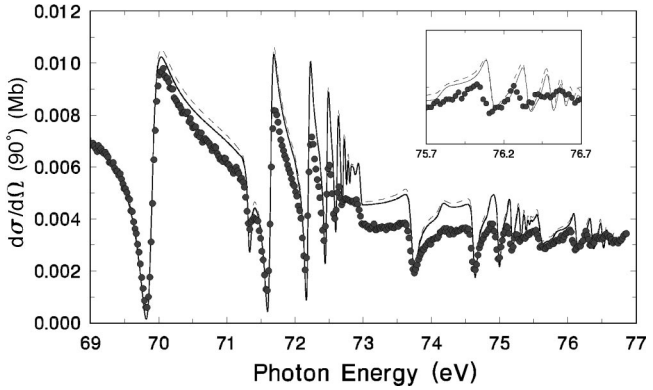

FIG. 2. Convoluted differential cross sections for photoionization into the $He^+(N=2)$ state at $\theta=90°$ at 69–76.8 eV employing Gaussian function with photon energy resolution (60 meV). Solid line, our results in the length form; dashed line, our results in the velocity form; solid circles, experimental data in Ref. [20].

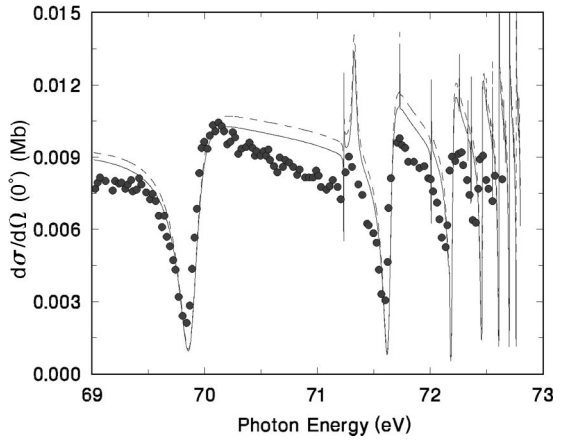

FIG. 3. Differential cross sections for photoionization into the $He^+(N=2)$ state at $\theta=0°$ at 69–73 eV. Solid line, our results in the length form; dashed line, our results in the velocity form; solid circles, experimental data in Ref. [21].

100 meV). There is good agreement with the series of resonance features classified as $4,2_n$ converging to the $He^+(N=4)$ limit in both spectra, with $n=4$ to 7 in the experiment and $n=4$ to 12 in present work. Comparing Figs. 5 and 6, the resonance features that can be seen in these two spectra have of course the same origin, but the line shapes and relative strengths are seen to depend strongly on the final states ($N=2$ or $N=3$). For the same resonance series, their magnitudes for photoionization to the $He^+(N=2)$ state are higher than those to the $He^+(N=3)$ state. However, some series such as $4,0_n$ can be shown more clearly in the spectra to the $N=3$ state than those to the $N=2$ state. Also, we notice from Fig. 6(a) that the $4,0_n$ states are clear in present calculations but only the $4,0_4$ state (at about 74.3 eV) is seen in the experiment [see Fig. 6(b)] due to the lower resolution. In general, the agreement of the partial DCS between the experiments and the present calculations is good from Figs. 5 and 6.

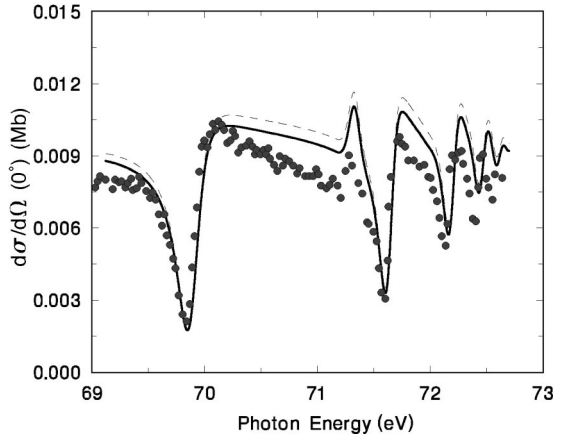

FIG. 4. Convoluted differential cross sections for photoionization into the $He^+(N=2)$ state at $\theta=0°$ at 69–73 eV employing Gaussian function with photon energy resolution (50 meV). Solid line, our results in the length form; dashed line, our results in the velocity form; solid circles, experimental data in Ref. [21].

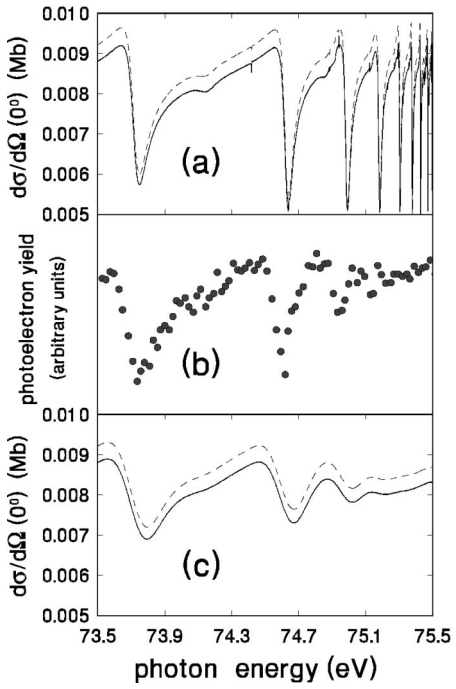

FIG. 5. Differential cross sections for photoionization into the $He^+(N=2)$ state at $\theta=0°$ at 73.5–75.5 eV. (a) Solid line, our results in the length form; dashed line, our results in the velocity form. (b) Relative experiment data in Ref. [21]. (c) Same as (a) but for convoluted results with resolution 100 meV.

The spectrum becomes very complex due to the strong interchannel interference resulting from nine correlated configurations between the $N=4$ and $N=5$ thresholds (76.0–76.8 eV). Thus, it is difficult to calculate accurately the

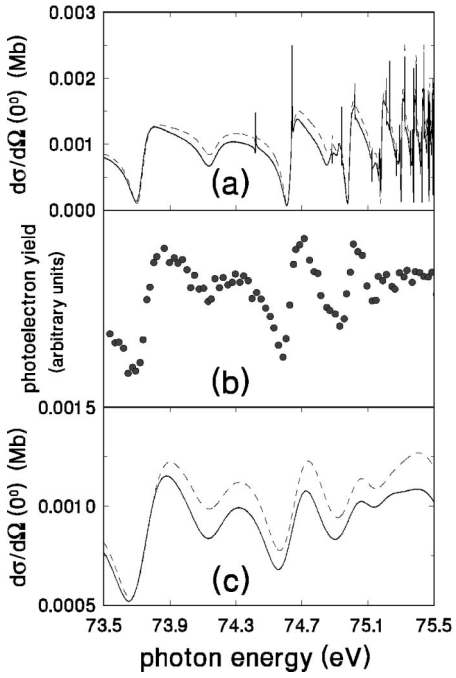

FIG. 6. Same as Fig. 5 but for photoionization cross sections into the $He^+(N=3)$ state.

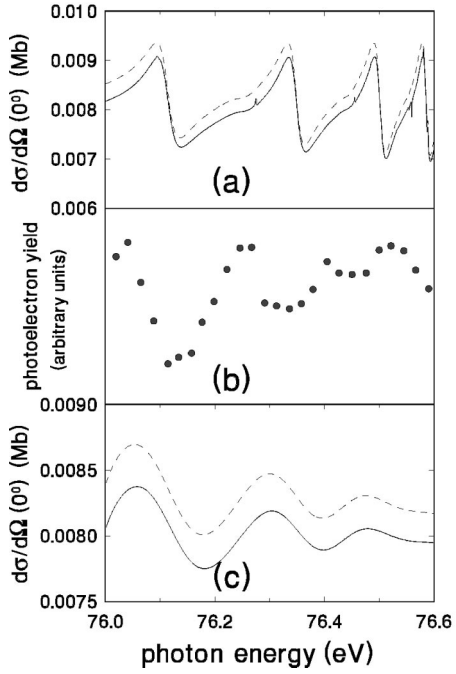

FIG. 7. Differential cross sections for photoionization into the $He^+(N=2)$ state at $\theta=0°$ at 76–76.6 eV. (a) Solid line, our results in the length form; dashed line, our results in the velocity form. (b) Relative experiment data in Ref. [21]. (c) Same as (a) but for convoluted results with resolution 100 meV.

photoionization spectra at higher photon energies due to the multitude of resonances and the perturbations by higher series (at the $N=6$ threshold), particularly in the DCS for photoinoization. The present calculations for the DCS of photoionization to the $N=2,3,4$ states of He^+ are plotted in Figs.

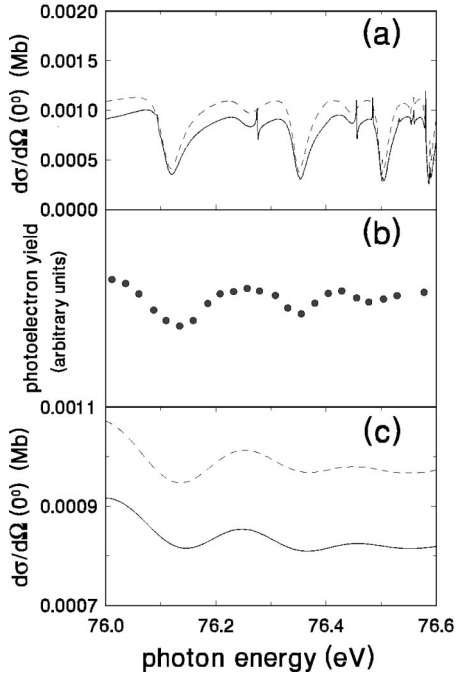

FIG. 8. Same as Fig. 7 but for photoionization cross sections into the $He^+(N=3)$ state.

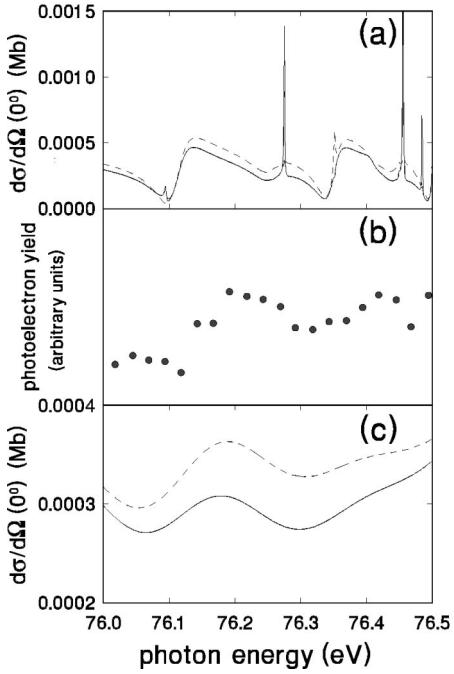

FIG. 9. Same as Fig. 7 but for photoionization cross sections into the $He^+(N=4)$ state at 76–76.5 eV.

7, 8, and 9 along with relative experimental measurements marked as (b) in these figures. It is noticeable that the resonance features $5,3_n$ show up most clearly in the $N=2$ and $N=3$ He^+ ion states in experiment, and compare well with our convoluted results. The magnitude of resonance states depends strongly on the He^+ ionic state and the magnitudes decrease as the states of the He^+ ion are varied from $N=2$ to 4 (see Figs. 7–9). Since the energy resolution is poor (100 meV), the present results in Figs. 7–9(a) present richer resonance structure than the experiments. For example, the $5,1_n$ resonance series, which are presented clearly in Figs. 7–9(a) using the present approach, cannot be seen in Zubek's experiments. We also notice that the shapes of the $5,1_n$ resonance series are different according to the different He^+ $N=2,3,4$ ionic states. Also, some differences in magnitude exist between our results in the length and velocity forms from Figs. 8–9. This is because the target functions and continuum orbitals included in the present approach are too few due to limited computational resources. In addition, there is a strong perturbation of the high-n $5,3_n$ Rydberg series by the lowest member of the next $6,4_6$ series (at about 76.6 eV) [5]. Thus, it makes the present results and the measurements of Zubek *et al.* differ above 76.45 eV since the present target functions do not include physical $6l$ orbitals. In addition, the lower energy resolution (100 meV) and less selected energies as well as relative measurements lead to difference in positions, widths and magnitudes of the $5,3_n$ states between the present convoluted results and the experimental data. We hope that more theoretical studies or higher resolution experiments will be undertaken in this energy region.

IV. CONCLUSIONS

The present *R*-matrix calculations include partial differential cross sections of photoionization from the ground state

$^1S^e$ to the final state $^1P^o$ leaving the $He^+(N)$ ion in the $N=2,3,4$ states between the $N=2$ and $N=5$ thresholds (69–76.8 eV). This energy range allows us to take account for the resonances due to excited states corresponding to $NLnl$ configurations. The quality of the target wave functions as well as bound and continuum ones for the $e+He^+$ system is ascertained by comparing the ionization energy I of He and the effective quantum numbers for the $^1S^e$ and $^1P^o$ states as well as the agreement of results in the length and velocity forms. In this study, we completed the calculation of partial differential cross sections of photoionization leaving He^+ in the $N=2$ state at $\theta=0°$ and 90° below the $N=3$ threshold. Compared with available theoretical and experimental results, good agreement is obtained. Between the $N=3$ and $N=5$ thresholds, we present theoretical values of partial DCS for photoionization leaving the He^+ ion in the $N=2,3,4$ levels. The agreement with experimental measurements is good. We notice that the present calculations provide rich resonance structure on the DCS for photoionization to the $He^+(N=2,3,4)$ states than available experiments with lower resolution 50–100 meV. No other comparable theoretical work exists in this energy region. Thus, we hope for more higher resolution experimental work and also more theoretical studies to check the present data of the DCS for photoionization. In addition, the discrepancy between length and velocity forms and between theory and experiment is also seen in the present paper. Additional pseudoorbitals will be required in this energy region near the double ionization threshold in order to converge the calculations. In future work, we will study in detail the widths, positions, Fano parameters, total cross sections, partial cross sections, partial asymmetry parameters, and branching ratios of autoionization resonance states from the $N=2$ to $N=5$ thresholds of He^+ ion.

ACKNOWLEDGMENT

This work is supported by the Natural Science and Education Foundation of Henan Province.

[1] P.R. Woodruff and J.A.R. Samson, Phys. Rev. Lett. **45**, 110 (1980).
[2] J.M. Bizau, F. Wuilleumier, P. Dhez, D.L. Ederer, T.N. Chang, S. Krummacher, and V. Schmidt, Phys. Rev. Lett. **48**, 588 (1982).
[3] D.W. Lindle, T.A. Ferrett, P.A. Heimann, and D.A. Shirley, Phys. Rev. A **36**, 2112 (1987).
[4] M. Domke, G. Remmers, and G. Kaindl, Phys. Rev. Lett. **69**, 1171 (1992).
[5] M. Domke, K. Schulz, G. Remmers, G. Kaindl, and D. Wintgen, Phys. Rev. A **53**, 1424 (1996).
[6] K. Schulz, G. Kaindl, M. Domke, J.D. Bozek, P.A. Heimann, A.S. Schlachter, and J.M. Rost, Phys. Rev. Lett. **77**, 3086 (1996).
[7] D.R. Herrick and O. Sinanoglu, Phys. Rev. A **11**, 97 (1975).
[8] R. Moccia and P. Spizzo, J. Phys. B **20**, 1423 (1987); Phys. Rev. A **43**, 2199 (1991).
[9] I. Sánchez and F. Martín, Phys. Rev. A **45**, 4468 (1992).
[10] T.N. Chang, Phys. Rev. A **47**, 3441 (1993); **47**, 705 (1993).
[11] C. Froese-Fischer and M. Idrees, J. Phys. B **23**, 679 (1990).
[12] P. Scott, P.G. Burke, W.C. Fon, and K.T. Taylor, J. Phys. B **15**, L603 (1982).
[13] K.A. Berrington, P.G. Burke, W.C. Fon, and K.T. Taylor, J. Phys. B **15**, L603 (1982).
[14] Y.K. Ho, Phys. Rev. A **44**, 4154 (1991).
[15] J.-Z. Tang, S. Watanable, and M. Matsuzawa, Phys. Rev. A **48**, 841 (1993); J.-Z. Tang, S. Watanable, M. Matsuzawa, C.D. Lin, Phys. Rev. Lett. **69**, 1633 (1992).
[16] B. Zhou and C.D. Lin, J. Phys. B **26**, 2575 (1993).
[17] T.W. Gorczyca and N.R. Badnell, J. Phys. B **30**, 3897 (1993).
[18] J. Yan, Y.Z. Qu, Lan VoKy, and J.M. Li, Phys. Rev. A **57**, 997 (1998).
[19] U. Fano, Rep. Prog. Phys. **46**, 97 (1983).
[20] M. Zubek, G. Dawber, R.I. Hall, L. Araldi, K. Ellis, and G.C. King, J. Phys. B **24**, L337 (1991).
[21] M. Zubek, G.C. King, P.M. Rutter, and F.H. Read, J. Phys. B **22**, 3411 (1989).
[22] P.G. Burke, A. Hibbert, and W.D. Robb, J. Phys. B **4**, 153 (1971).
[23] K.A. Berrington, P.G. Burke, J.I. Chang, A.T. Chivers, W.D. Robb, and K.T. Taylor, Comput. Phys. Commun. **8**, 149 (1974).
[24] K.A. Berrington, P.G. Burke, M. Le Dourneuf, W.D. Robb, K.T. Taylor, and Lan VoKy, Comput. Phys. Commun. **14**, 346 (1978).
[25] K.A. Berrington, P.G. Burke, K. Butler, M.J. Seaton, P.J. Storey, K.T. Taylor, and Y. Yu, J. Phys. B **20**, 6379 (1987).
[26] E. Clementi and R. Roetti, At. Data Nucl. Data Tables **14**, 177 (1974).
[27] M. Le Dourneuf (unpublished); Vo Ky Lan, M. Le Dourneuf, and P.G. Burke, J. Phys. B **9**, 1065 (1976).
[28] C.L. Pekeris, Phys. Rev. **162**, 1470 (1962).
[29] J. Mcl. Calvert and W.D. Davison, J. Phys. B **4**, 314 (1971).
[30] J.A. Fernley, K.T. Taylor, and M.J. Seaton, J. Phys. B **20**, 6457 (1987).
[31] C.L. Pekeris, Phys. Rev. **126**, 1470 (1962).
[32] D.R. Herrick and O. Sinanoglu, Phys. Rev. A **11**, 97 (1975).
[33] C.E. Moore, *Atomic Energy Levels I* (U.S. GPO, Washington, 1971).